MATERIALS PHYSICS AND MECHANICS RESEARCH ARTICLE

Submitted: July 24, 2024 Revised: October 30, 2024 Accepted: November 29, 2024

Fractional strain analysis on reflection of plane waves at an impedance boundary of non-local swelling porous thermoelastic medium

S. Sharma [1], D. Batra [2]✉, R. Kumar [3]

[1] Houston University, Houston, USA

[2] Kishan Lal Public College, Rewari, Haryana, India

[3] Kurukshetra University, Kurukshetra, Haryana, India

✉ divyabatra1982@gmail.com

ABSTRACT

The current work focuses on developing a model to examine wave analysis in non-local swelling porous thermoelastic medium under fractional order strain. After converting the governing equations into two-dimensional and utilizing the dimensionless quantities for further simplification the Helmholtz decomposition theorem has been used to decompose the system into longitudinal and transverse components. The frequency dispersion relation is derived by assuming the plane wave solution in two-dimensional case for the given problem. It is found that there exist two dilatational waves, a thermal wave and two transversal waves travelling at distinct velocities. The amplitude ratios for the reflected waves are obtained with the aid of impedance boundary restrictions. The obtained amplitude ratios are used to obtain the energy ratios of different reflected waves. Influence of fractional order parameter on distinct types of wave speeds is illustrated graphically and it is observed that increase in fractional order parameter diminishes the magnitude of all existing waves except longitudinal wave in solid. Also impacts of swelling pores and fractional order on the attained energy ratios are displayed graphically versus angle of incidence. It is verified that during reflection phenomena, the sum of energy ratio is equal to unity at each angle of incidence and there is no dissipation on the boundary surface. Swelling porosity decrease the impact of energy ratios of reflected longitudinal wave and thermal wave for all values of fractional order parameter. Some unique cases are also presented. The results find application in geophysics, civil engineering and structure related issues.

KEYWORDS

energy ratios • reflection coefficients • impedance border • fractional order strain • swelling porous

Citation: Sharma S, Batra D, Kumar R. Fractional strain analysis on reflection of plane waves at an impedance boundary of non-local swelling porous thermoelastic medium. *Materials Physics and Mechanics*. 2025;53(1): 1–21.

http://dx.doi.org/10.18149/MPM.5312025_1

Introduction

As wave phenomena have numerous applications in the field of geophysics, civil engineering, oil exploration, slurry, and agriculture scientists and researchers have long been very interested in studying wave phenomena in porous media. The model of wave circulation in fluid-saturated porous solids and the identification of the presence of lower and higher frequency ranges were initially presented by Biot [1,2]. Eringen [3] acknowledged the utility of mixture theory in the area of expanding porous elastic media. He used a combination of elastic solid, viscous liquid, and gas in his work and focused on things like soil swelling, wood, paper, and fiber drying, among other things. Subsequently, other researchers have made contributions to the topic of porous elastic media swelling. The amplitude ratios resulting from plane wave reflection and transmission at the border of thermoelastic swelling porous media were determined by Kumar et al. [4].

Margin and Royston [5] being the first to propose the fractional order strain model that can both predict mechanical deformation of Hookean solid and Newtonian fluid by using zero-order and one-order derivative. More significantly fractional order parameter of fractional order strain model can be chosen freely within the range 0–1 according to the necessity of practical application. In recent year one can find that the concept of fractional order strain has been successfully used in thermomechanical analysis of elastic and dipolar material systems [6–10]. Moreover, global dependency and non-local property of the fractional derivative is one of the main reason for its increasing popularity. The concept of non-linearity using fractional differential operator in thermoelastic models opens up a new perspective on the study of thermoelastic deformation in solid mechanics. A significant contribution in the theory of thermoelasticity with non-locality can be found in [11–15]. Vlase et al. [16] determined the properties of eigen values for transverse and torsional vibrations in a mechanical system having two identical beams. Sharma et al. [17] examined basic theorems and plane wave in thermoelastic diffusion using multiphase lag model with temperature dependence. Relaxed Saint-Venant principle for thermoelastic micropolar diffusion is given by Marin et al. [18].

The reflection of plane waves in thermodiffusive elastic half-space with voids was investigated by [19]. Wave propagating in a micropolar thermoelastic medium with two temperatures and layers of half-spaces surrounded by an inviscid liquid was investigated by Sharma et al. [20]. In micropolar elastic materials, plane wave reflection and transmission were investigated by Sharma et al. [21,22]. The Rayleigh wave propagation in incompressible anisotropic half spaces with impedance boundary conditions was studied by Vinh and Hue [23]. Kumar and Sharma [24] developed uniqueness, reciprocity theorems, and variational principle in piezothermoelastic medium having fractional order derivative. Sharma and Khator [25,26] looked at a few issues related to the production of electricity from renewable sources. In a modified Green-Lindsay theory, Kumar et al. [27] investigated the effect of impedance factors on wave propagation in a micropolar thermoelastic medium. According to Singh and Kaur [28], when micropolar parameters grow, so does the influence of impedance parameters. Amin et al. [29] used fractional relaxation operators and studied the response of laser irradiation in viscoelastic thin film of metal. Kaushal et al. [30] studied the impact of stiffness and void when waves propagate through non-free surface and free surface.

Ezzat and Lewis [31] used fractional thermos viscoelasticity to study head induced mechanical response in human skin tissue. Amin et al. [32] constructed thermoviscoelastic metal film with fractional relaxation operators and studied the microscale response using laser pulse heat flux with non-Gaussian form. Ezzat and Muhiameed [33] studied the response of non-local size dependent piezoelectric materials in thermoviscoelastic theory. Ezzat [34,35] used state space approach to develop non-local thermo-viscoelastic model and studied the response of piezoelectric materials with fractional dual phase heat transfer. Yadav et al. [36] investigation on nonlocal porous thermo-micropolar diffusive medium revealed that both diffusion and porous properties have no effect on transversal waves. When Kumar [37] examined the effect of fractional derivative on wave propagation using Eringen's non-local approach, he discovered that group speed decreased as elastic medium values increased.

Abouelregal et al. [38] studied the impact of non-local Moore Gibson Thompson on thermoelastic material under the model of memory dependent derivatives. Abouelregal et al. [39] used Eringen's non-local thermoelastic theory and studied changes in heat transfer in thermoelastic materials under initial stress. Alsaeed [40] used Atangana Baleanu fractional derivative and analysed magneto thermoelastic response in unbounded porous body in context of dual phase lag model. Abouelregal et al. [41] used fractional model for one dimensional non-local elasticity theory and studied the transfer of heat flow through nanomaterials. Non-local parameters enhances the amplitude ratios when longitudinal and thermal waves are incident in generalized thermoelastic medium with two temperature and impedance parameters [42]. Ezzat and Bary [43] used memory dependent derivative to investigate the problem of wave characteristics in thermoelectric viscoelastic solid. Yadav [44] investigated how the magneto-thermo-microstretch half space having an impedance boundary's diffusion parameter and fractional order parameter affected the reflection coefficients of plane waves. Elhagary [45] investigated the impact of fractional derivative on thermoelastic diffusive half-space using the integral transform technique. Alruwaili et al. [46] used new form of fractal form of Green-Naghdi theory and developed a mathematical model of thermoelectric MHD theory. Kumar et al. [47] studied the reflection of waves through swelling porous thermoelastic half space having boundary under dual phase lag model.

The purpose of this work is to examine wave analysis in nonlocal swelling porous thermoelastic medium and found that there exist three longitudinal waves namely *Ps*, *Pf*, *T* waves and two transverse waves *SVS*, and *SVF* waves. Impedance boundary restrictions are used to obtain the amplitude ratios and energy ratios of various reflected waves. Numerical calculations and graphical representation are also used to examine the effect of variation in fractional order strain and swelling porosity in energy ratios.

Methods

Basic Equations

In swelling porous thermoelastic medium basic equations in absence of body force is given as [3]:

$$\begin{aligned}&\mu(1+\tau^r D_1^r)u^s_{i,jj}+(\lambda+\mu)(1+\tau^r D_1^r)u^s_{j,ji}-\sigma^f(1+\tau^r D_1^r)u^f_{j,ji}+\xi^{ff}\left(\dot{u}^f_i-\dot{u}^s_i\right)+\\&+\left(\gamma^f-\alpha_0\right)\nabla T=\rho_0^s(1-\xi_1^2\nabla^2)\ddot{u}^s_i\,,\end{aligned} \tag{1}$$

$$\begin{aligned}&\mu_v(1+\tau^r D_1^r)\dot{u}^f_{i,jj}+(\lambda_v+\mu_v)(1+\tau^r D_1^r)\dot{u}^f_{j,ji}-\sigma^f(1+\tau^r D_1^r)u^s_{j,ji}-\\&-\sigma^{ff}(1+\tau^r D_1^r)u^f_{j,ji}-\xi^{ff}\left(\dot{u}^f_i-\dot{u}^s_i\right)-\left(\gamma^f+\alpha^f\right)\nabla T=\rho_0^f(1-\xi_2^2\nabla^2)\ddot{u}^f_i,\end{aligned} \tag{2}$$

$$(1+\tau^r D_1^r)\nabla.\dot{u}^f\left(\alpha^f+\frac{\zeta^f}{T_0}\right)+(1+\tau^r D_1^r)\nabla.\dot{u}^s\left(\alpha_0+\frac{\zeta^f}{T_0}\right)+\alpha_1\dot{T}-\frac{K^*}{T_0}\nabla^2 T=0, \tag{3}$$

$$t^s_{ij}=\left(-\alpha_0 T-\sigma^f(1+\tau^r D_1^r)u^f_{r,r}+\lambda(1+\tau^r D_1^r)u^s_{r,r}\right)\delta_{ij}+\mu(1+\tau^r D_1^r)(u^s_{i,j}+u^s_{j,i}), \tag{4}$$

$$\begin{aligned}&t^f_{ij}=\left(-\alpha^f T-\sigma^f(1+\tau^r D_1^r)u^s_{r,r}-\sigma^{ff}(1+\tau^r D_1^r)\nabla.u^f+\lambda_v(1+\tau^r D_1^r)\dot{u}^f_{r,r}\right)\delta_{ij}+\\&+\mu_v(u^f_{i,j}+u^f_{j,i}),\end{aligned} \tag{5}$$

where s is a solid, f is a fluid, u_i^s, u_i^f are the displacement components of a solid and a liquid, respectively, ρ_0^s, ρ_0^f are the densities in a solid and a liquid respectively, λ, μ, λ_v, μ_v, σ^f, σ^{ff}, ξ^{ff} are the constitutive constants, α_1, ζ^f, α^f, α_0 are the material constants, ξ_1, ξ_2 are the non-local parameters, r is an order of fractional strain, T is a temperature and K^* is a thermal conductivity, t_{ij}^s, t_{ij}^f are the partial stress tensors.

Problem Statement and Simplification

We have considered an isotropic, homogeneous swelling porous thermoelastic half-space. The origin of the rectangular cartesian co-ordinate system (x_1, x_2, x_3) is taken at boundary $x_3 = 0$ with x_3 − axis is pointing normally into medium (Fig. 1). The x_2 − axis is an intersection of the plane's wavefront and the plane surface. We confine our study to plane strain problem parallel to $x_1 - x_3$ plane. For two-dimensional problem, we take:

$$u^k = \left(u_1^k, 0, u_3^k\right);\ k = s, f. \tag{6}$$

Define dimensionless quantities as:

$$x_i' = \frac{\omega^*}{c_1}x_i, u_i^{k\prime} = \frac{\rho_0^S\omega^*c_1}{\alpha_0 T_0}u_i^k, t_{ij}^{k\prime} = \frac{t_{ij}^k}{\alpha_0 T_0}, T' = \frac{T}{T_0}, \xi_m' = \frac{\omega^*}{c_1}\xi_m, t' = \omega^* t, \omega' = \frac{\omega}{\omega^*},$$
$$\tau^{r\prime} = \omega^{*r}\tau^r, \xi_m' = \frac{\omega^*}{c_1}\xi_m, \tau^{r\prime} = \omega^{*r}\tau^r, z_l' = \frac{z_l}{\rho_0^S c_1}, z_5' = \frac{c_1}{K^*}z_5, \omega^* = \frac{\alpha_1 T_0 c_1^2}{K^*}, c_1^2 = \frac{\lambda+2\mu}{\rho_0^S}, \tag{7}$$

where m = 1, 2; k = s, f; i, j = 1, 2, 3; l = 1, 2, 3, 4.

Using Helmholtz decomposition, displacement components $u_1^k(x_1, x_3, t)$, $u_3^k(x_1, x_3, t)$ are related to potentials ϕ and ψ as:

$$u_1^k = \frac{\partial\phi^k}{\partial x_1} - \frac{\partial\psi^k}{\partial x_3}, u_3^k = \frac{\partial\phi^k}{\partial x_3} + \frac{\partial\psi^k}{\partial x_1}. \tag{8}$$

Equations (1)−(3) with the help of Eqs. (6)−(8) becomes:

$$\left(P\nabla^2 - a_2\frac{\partial}{\partial t} - (1 - \xi_1^2\nabla^2)\frac{\partial^2}{\partial t^2}\right)\phi^s + \left(-a_1 P\nabla^2 + a_2\frac{\partial}{\partial t}\right)\phi^f - a_3 T = 0, \tag{9}$$

$$\left(-\delta_1^2 P\nabla^2 + a_2\frac{\partial}{\partial t} + (1 - \xi_1^2\nabla^2)\frac{\partial^2}{\partial t^2}\right)\psi^s - a_2\frac{\partial}{\partial t}\psi^f = 0, \tag{10}$$

$$\left(-h_1 P\nabla^2 + h_3\frac{\partial}{\partial t}\right)\phi^s + \left(P\frac{\partial}{\partial t}\nabla^2 - h_2 P\nabla^2 - h_3\frac{\partial}{\partial t} - h_5(1 - \xi_2^2\nabla^2)\frac{\partial^2}{\partial t^2}\right)\phi^f - h_4 T = 0, \tag{11}$$

$$\left(-h_3\frac{\partial}{\partial t}\right)\psi^s + \left(-\delta_2^2 P\nabla^2\frac{\partial}{\partial t} + h_3\frac{\partial}{\partial t} - h_5(1 - \xi_2^2\nabla^2)\frac{\partial^2}{\partial t^2}\right)\psi^f = 0, \tag{12}$$

$$\left(b_3 P\nabla^2\frac{\partial}{\partial t}\right)\phi^s + \left(b_2 P\nabla^2\frac{\partial}{\partial t}\right)\phi^f + \phi^f + \left(\frac{\partial}{\partial t} - \nabla^2\right)T = 0, \tag{13}$$

where $\delta_1^2 = \frac{\mu}{\lambda+2\mu}$, $a_1 = \frac{\sigma^f}{\lambda+2\mu}$, $a_2 = \frac{\xi^{ff}}{\rho_0^S\omega^*}$, $a_4 = \frac{\lambda}{\lambda+2\mu}$, $a_3 = (1 - \tau_0)$, $\tau_0 = \frac{\gamma^f}{\alpha_0}$, $\beta_1 = \alpha_0 T_0 + \zeta^f$,
$\delta_2^2 = \frac{\mu_v}{\lambda_v+2\mu_v}$, $h_1 = \frac{\sigma^f}{\omega^*(\lambda_v+2\mu_v)}$, $h_2 = \frac{\sigma^{ff}}{\omega^*(\lambda_v+2\mu_v)}$, $h_3 = \frac{\xi^{ff}c_1^2}{\omega^{*2}(\lambda_v+2\mu_v)}$, $\beta_2 = \alpha^f T_0 + \zeta^f$,
$h_4 = \frac{(1+\tau_1)\alpha^f\rho_0^S c_1^2}{\omega^*\alpha_0(\lambda_v+2\mu_v)}$, $h_5 = \frac{\rho_0^f c_1^2}{\omega^*(\lambda_v+2\mu_v)}$, $\tau_1 = \frac{\gamma^f}{\alpha^f}$, $b_2 = \frac{\alpha_0\beta_2}{\rho_0^S c_1^2\alpha_1 T_0}$, $b_3 = \frac{\alpha_0\beta_1}{\rho_0^S c_1^2\alpha_1 T_0}$, $\nabla^2 = \left(\frac{\partial^2}{\partial x_1^2} + \frac{\partial^2}{\partial x_3^2}\right)$,
$P = 1 + \tau^r(-i\omega)^r$.

Considering the motion to be time harmonic we assume:

$$(\phi^s, \phi^f, T, \psi^s, \psi^f) = (\bar{\phi}^s, \bar{\phi}^f, \bar{T}, \bar{\psi}^s, \bar{\psi}^f)e^{i\{k(x_1 sin\theta - x_3 cos\theta) - \omega t\}}, \tag{14}$$

where θ is the angle of inclination; k is a wave number.

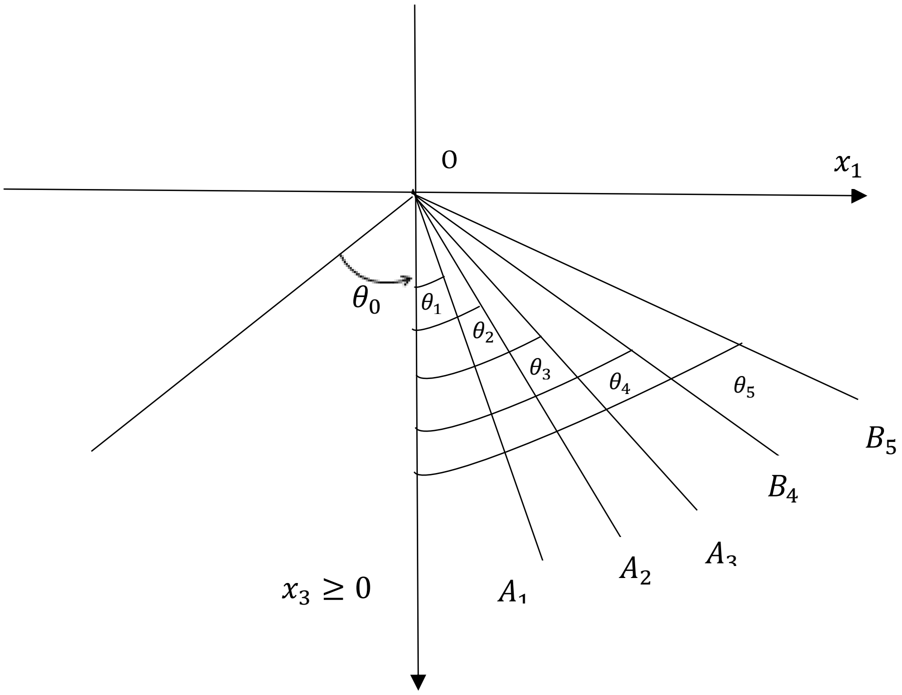

Fig. 1. Geometry of the problem depicting incident and reflected waves in swelling porous thermoelastic half-space

Making use of Eq. (14) in Eqs. (9)–(13), we obtain

$$Av^6 + Bv^4 + Cv^2 + D = 0, \tag{15}$$

$$A_1v^4 + B_1v^2 + C_1 = 0, \tag{16}$$

where $v_i(i = 1, 2, 3)$ are the roots of Eq. (15) correspond to velocity of *Ps*-wave, *Pf*-wave and *T*-wave whereas $v_j(j = 4, 5)$ are the roots of Eq. (16) giving velocity of *SVS*-wave and *SVF*-wave: $A = \tau_{12}\tau_{24} - \tau_{11}\tau_{21}, B = P_1\tau_{24} + d_1\tau_{12} + Pa_1\tau_{21} + d_3\tau_{11} + d_5\tau_{13},\ D = P_1d_2 + Pa_1d_4,$
$C = P_1d_1 + d_2\tau_{12} + Pa_1d_3 + d_4\tau_{11} + d_6\tau_{13}, A_1 = \tau_{44}\tau_{43} - \tau_{11}\tau_{21},\ B_1 = \tau_{41}\tau_{43} + \tau_{44}\tau_{42},$
$C_1 = \tau_{41}\tau_{42}, P_1 = -P + \xi_1^2\omega^2,\ \tau_{11} = \frac{ia_2}{\omega}, \tau_{13} = \frac{-a_2}{\omega^2}, \tau_{12} = 1 + \tau_{11},\ \tau_{21} = \frac{ih_3}{\omega}, \tau_{23} = \frac{-h_4}{\omega^2},$
$\tau_{22} = P(i\omega + h_2) + h_5\xi_2^2\omega^2,\ \tau_{24} = h_5 + \tau_{21}, \tau_{31} = -b_3\omega^2P,\ \tau_{32} = -b_2\omega^2P,$
$d_1 = \tau_{22-}\tau_{32}\tau_{23},\ d_2 = (\tau_{22+}\tau_{24})i\omega, d_3 = Ph_1 - \tau_{21}i\omega - \tau_{31}\tau_{23}, d_4 = Ph_1i\omega, \tau_{43} = h_5 - \tau_{21},$
$d_5 = -(\tau_{21}\tau_{32} + \tau_{31}\tau_{24}),\ d_6 = Ph_1\tau_{32} - \tau_{31}\tau_{22}, \tau_{41} = \delta_1^2P - 1,\ \tau_{44} = -(\xi_1^2 + \tau_{11}),$
$\tau_{42} = -P\delta_2^2i\omega + h_5\xi_2^2\omega^2.$

Making use of Eqs. (6)–(8) in Eqs. (4)–(5) we obtain:

$$t_{33}^s = (1 + \tau^r D_1^r)\left(-a_1\left(\frac{\partial^2\phi^f}{\partial x_1^2} + \frac{\partial^2\phi^f}{\partial x_3^2}\right) + a_4\left(\frac{\partial^2\phi^s}{\partial x_1^2} + \frac{\partial^2\phi^s}{\partial x_3^2}\right) + 2\delta_1^2\left(\frac{\partial^2\phi^s}{\partial x_3^2} + \frac{\partial^2\psi^s}{\partial x_3\partial x_1}\right)\right), \tag{17}$$

$$t_{31}^s = \delta_1^2(1 + \tau^r D_1^r)\left(2\frac{\partial^2\phi^s}{\partial x_3\partial x_1} + \frac{\partial^2\psi^s}{\partial x_1^2} - \frac{\partial^2\psi^s}{\partial x_3^2}\right), \tag{18}$$

$$t_{33}^f = (1 + \tau^r D_1^r)\left(-a_1\left(\frac{\partial^2\phi^s}{\partial x_1^2} + \frac{\partial^2\phi^s}{\partial x_3^2}\right) - e_1\left(\frac{\partial^2\phi^f}{\partial x_1^2} + \frac{\partial^2\phi^f}{\partial x_3^2}\right) + e_2\left(\frac{\partial^2\dot\phi^f}{\partial x_1^2} + \frac{\partial^2\dot\phi^f}{\partial x_3^2}\right) + \right.$$
$$\left. +2e_3\omega^*\left(\frac{\partial^2\dot\phi^f}{\partial x_3^2} + \frac{\partial^2\dot\psi^f}{\partial x_3\partial x_1}\right)\right) - \tau_2T, \tag{19}$$

$$t_{31}^f = e_3\omega^*(1 + \tau^r D_1^r)\left(2\frac{\partial^2\dot\phi^f}{\partial x_3\partial x_1} + \frac{\partial^2\dot\psi^f}{\partial x_1^2} - \frac{\partial^2\dot\psi^f}{\partial x_3^2}\right), \tag{20}$$

where $\tau_2 = \frac{\alpha^f}{\alpha_0},\ e_1 = \frac{\sigma^{ff}}{\lambda+2\mu}, e_2 = \frac{\lambda_v\omega^*}{\lambda+2\mu}, e_3 = \frac{\mu_v}{\lambda+2\mu}.$

Boundary conditions

Relevant boundary conditions at surface $x_3 = 0$ are:

$$\text{(i) } t_{33}^{s} + \omega z_1 u_3^{s} = 0, \text{ (ii) } t_{31}^{s} + \omega z_2 u_1^{s} = 0, \quad \text{(iii) } t_{33}^{f} + \omega z_3 u_3^{f} = 0,$$
$$\text{(iv) } t_{31}^{f} + \omega z_4 u_1^{f} = 0, \text{ (v) } K^{*}\frac{\partial T}{\partial x_3} + \omega z_5 T = 0, \tag{21}$$

where z_1, z_2, z_3, z_4 are impedance parameters having dimension $\frac{Ns}{m^3}$; z_5 is impedance parameter having dimension $\frac{N}{mK}$.

We assume the values of $\phi^s, \phi^f, T, \psi^s, \psi^f$ as:

$$\phi^s = \sum A_{0i} e^{i\{k(x_1 sin\theta_0 - x_3 cos\theta_0) - \omega t\}} + A_i e^{i\{k(x_1 sin\theta_i + x_3 cos\theta_i) - \omega t\}}, \tag{22}$$

$$\phi^f = \sum \alpha_i (A_{0i} e^{i\{k(x_1 sin\theta_0 - x_3 cos\theta_0) - \omega t\}} + A_i e^{i\{k(x_1 sin\theta_i + x_3 cos\theta_i) - \omega t\}}), \tag{23}$$

$$T = \sum \beta_i (A_{0i} e^{i\{k(x_1 sin\theta_0 - x_3 cos\theta_0) - \omega t\}} + A_i e^{i\{k(x_1 sin\theta_i + x_3 cos\theta_i) - \omega t\}}), \tag{24}$$

$$\psi^s = \sum B_{0j} e^{i\{k(x_1 sin\theta_0 - x_3 cos\theta_0) - \omega t\}} + B_j e^{i\{k(x_1 sin\theta_j + x_3 cos\theta_j) - \omega t\}}, \tag{25}$$

$$\psi^f = \sum \gamma_j (B_{0j} e^{i\{k(x_1 sin\theta_0 - x_3 cos\theta_0) - \omega t\}} + B_j e^{i\{k(x_1 sin\theta_j + x_3 cos\theta_j) - \omega t\}}), \tag{26}$$

where $\alpha_i = \frac{-\tau_{23}V^2(P_1+\tau_{12}V^2)+\tau_{13}V^2(h_1P-\tau_{21}V^2)}{(a_1P-\tau_{11}V^2)\tau_{23}V^2-\tau_{13}V^2(\tau_{22}+\tau_{24}V^2)}$, $\beta_i = \frac{(\tau_{22}+\tau_{24}V^2)(P_1+\tau_{12}V^2)-(a_1P-\tau_{11}V^2)(h_1P-\tau_{21}V^2)}{(a_1P-\tau_{11}V^2)\tau_{23}V^2-\tau_{13}V^2(\tau_{22}+\tau_{24}V^2)}$, $\gamma_j = \frac{\tau_{41}+\tau_{44}V^2}{-\tau_{11}V^2}$, *(i*=1,2,3*; j*=3,4*)*.

Here $A_{0i}(i = 1, 2, 3)$ denote amplitude of incident *Ps*-wave, *Pf*-wave and *T*-wave $A_i(i = 1, 2, 3)$ correspond to reflected *Ps*-wave, *Pf*-wave and *T*-wave; $B_{0j}(j = 3, 4)$ correspond to amplitude of incident *SVS*-wave and *SVF*-wave and $B_j(j = 3, 4)$ associate to reflected *SVS*-wave and *SVF*-wave.

Snell's Law is represented as $\frac{sin\theta_0}{v_0} = \frac{sin\theta_i}{v_i}$ *(i=1, 2, 3, 4, 5)*, where $k_1 v_1 = k_2 v_2 = = k_3 v_3 = k_4 v_4 = k_5 v_5 = \omega$. Using Eqs. (8), (17)–(20) in boundary conditions (21) we obtain the following relation coefficients (or amplitude ratios):

$$\sum a_{pj} Z_j = g_p, \; (p, j = 1, 2, 3, 4, 5), \tag{27}$$

where

$$a_{1i} = \left[P\left(\alpha_i a_1 - a_4 - 2\delta_1^2\left(1 - \left(\frac{v_i}{v_1}\right)^2 sin^2\theta_0\right)\right) - \frac{\beta_i}{k_i^2}\right]\left(\frac{v_1}{v_i}\right)^2 + \frac{v_1^2}{v_i} z_1 \sqrt{1 - \left(\frac{v_i}{v_1}\right)^2 sin^2\theta_0},$$

$$g_1 = P(\alpha_1 a_1 - a_4 - 2\delta_1^2 cos^2\theta_0) - \frac{\beta_1}{k_1^2} + v_1 z_1 i cos\theta_0,$$

$$a_{1j} = P\left(-2\delta_1^2 sin\theta_0 \sqrt{1 - \left(\frac{v_j}{v_1}\right)^2 sin^2\theta_0}\right)\left(\frac{v_1}{v_j}\right) + i z_1 v_1 sin\theta_0,$$

$$a_{2i} = P\left(-2\delta_1^2 sin\theta_0 \sqrt{1 - \left(\frac{v_j}{v_1}\right)^2 sin^2\theta_0}\right)\left(\frac{v_1}{v_i}\right) + i z_2 v_1 sin\theta_0,$$

$$a_{2j} = P\delta_1^2\left(-\left(\frac{v_j}{v_1}\right)^2 sin^2\theta_0 + \left(1 - \left(\frac{v_j}{v_1}\right)^2 sin^2\theta_0\right)\right)\left(\frac{v_1}{v_j}\right)^2 - \frac{v_1^2}{v_j} i z_2 \sqrt{1 - \left(\frac{v_j}{v_1}\right)^2 sin^2\theta_0},$$

$$g_2 = P(-2\delta_1^2 sin\theta_0 cos\theta_0) - i z_2 v_1 sin\theta_0,$$

$$a_{3i} = \left[P\left(a_1 + e_1\alpha_i + i k_i v_i \alpha_i\left(e_2 + 2e_3\omega^*\left(1 - \left(\frac{v_i}{v_1}\right)^2 sin^2\theta_0\right)\right)\right) - \frac{\tau_2\beta_i}{k_i^2}\right]\left(\frac{v_1}{v_i}\right)^2 +$$
$$+ i\alpha_i z_3 \frac{v_1^2}{v_i}\sqrt{1 - \left(\frac{v_i}{v_1}\right)^2 sin^2\theta_0},$$

$$g_3 = -P(a_1 + e_1\alpha_1 + i k_1 v_1 \alpha_1(e_2 + 2e_3\omega^* cos^2\theta_0)) + \frac{\tau_2\beta_i}{k_1^2} + v_1 z_3 \alpha_1 i cos\theta_0,$$

$$a_{3j} = i k_j \gamma_j 2 P e_3 \omega^* v_1 sin\theta_0 \sqrt{1 - \left(\frac{v_j}{v_1}\right)^2 sin^2\theta_0} + i z_3 \gamma_j v_1 sin\theta_0,$$

$a_{4i} = ik_i\alpha_i 2Pe_3\omega^* v_1 sin\theta_0\sqrt{1-\left(\frac{v_i}{v_1}\right)^2 sin^2\theta_0} + i\frac{v_1^2}{v_i}z_4\alpha_i sin\theta_0,$
$g_4 = ik_1\alpha_1 2Pe_3\omega^* v_1 sin\theta_0 cos\theta_0 - iv_1 z_4\alpha_1 sin\theta_0,$
$a_{4j} = \left[Pe_3\omega^*\left(ik_j\gamma_j v_j sin^2\theta_0 + \left(1-\left(\frac{v_j}{v_1}\right)^2 sin^2\theta_0\right)\left(-ik_j\gamma_j\frac{v_1^2}{v_j}\right)\right)\right] - iz_4\gamma_j\frac{v_1^2}{v_j}\sqrt{1-\left(\frac{v_j}{v_1}\right)^2 sin^2\theta_0},$
$a_{5i} = iK^*\frac{\beta_i}{k_i}\left(\frac{v_1}{v_i}\right)^2\sqrt{1-\left(\frac{v_i}{v_1}\right)^2 sin^2\theta_0} + z_5\frac{\beta_i}{k_i}\frac{v_1^2}{v_i}, g_5 = iK^*\frac{\beta_1}{k_1}cos\theta_0 - z_5\frac{\beta_1}{k_1}v_1, a_{54} = a_{55} = 0,$
where $Z_i = \frac{A_i}{A_{01}}$ (*I = 1, 2, 3*) and $Z_j = \frac{B_j}{A_{01}}$ ($j = 4, 5$) are the amplitude ratios of reflected *Ps, Pf, T* and *SVS, SVF* waves respectively for an incident *Ps* wave.

Similarly, amplitude ratios of reflected waves can be calculated for the incident *Pf* or *T* or *SVS* or *SVF* waves.

Energy ratios of reflected waves

In this section the partition of energy among different reflected waves is calculated. Following Achenbach [48], the rate at which the energy is transmitted per unit surface area per unit time is expressed as:

$$P^e = \frac{1}{2}\sum_{k=s,f}\Re\left((t_{33}^k)\dot{\tilde{u}}_3^k)\right) + \frac{1}{2}\sum_{k=s,f}\Re\left(\left(t_{31}^k\right)\left(\dot{\tilde{u}}_1^k\right)\right). \tag{28}$$

The average reflected wave energy at $x_3 = 0$ is given by:

$$|E_i| = -\left(\frac{A_i}{A_{01}}\right)^2\frac{\left(\frac{v_1}{v_i}\right)^2\sqrt{1-\left(\frac{v_i}{v_1}\right)^2 sin^2\theta_0}\left[P(\alpha_i a_1 - a_4 - 2\delta_1^2) - \frac{\beta_i}{k_i^2} + r_i\right]}{cos\theta_0\left[P(\alpha_1 a_1 - a_4 - 2\delta_1^2) - \frac{\beta_1}{k_1^2} + r_1\right]}, \tag{29}$$

$$|E_j| = -\left(\frac{B_j}{A_{01}}\right)^2\frac{\left(\frac{v_1}{v_j}\right)^2\sqrt{1-\left(\frac{v_j}{v_1}\right)^2 sin^2\theta_0}\left(P(-\delta_1^2 + i\omega e_3\omega^*\gamma_j^2)\right)}{cos\theta_0\left[P(\alpha_1 a_1 - a_4 - 2\delta_1^2) - \frac{\beta_1}{k_1^2} + r_1\right]}, \tag{30}$$

where, $r_i = \alpha_i P(a_1 + e_1\alpha_i + ik_i\alpha_i v_i e_2 + 2ie_3\omega^* k_i\alpha_i) - \frac{\tau_2\beta_i}{k_i^2}$, *(I = 1, 2, 3; j = 4, 5).*

Numerical results and Discussion

In order to demonstrate the impact of impedance parameter at various values of fractional order differential parameters on energy ratios of reflected *Ps, Pf, T, SVS* and *SVF* waves the following data is taken [47] (Table 1).

Table 1. Various values of fractional order differential parameters on energy ratios of reflected Ps, Pf, T, SVS and SVF waves

Symbol	Value	Symbol	Value
λ, N/m²	$6.0\cdot 10^9$	α^f, N/m² K	$0.152\cdot 10^6$
μ, N/m²	$9.0\cdot 10^9$	α_0, N/m² K	$0.015\cdot 10^6$
λ_v, Ns/m²	$1.002\cdot 10^{-3}$	K^*, N/sK	$0.498\cdot 10^2$
μ_v, Ns/m²	$8.88\cdot 10^{-4}$	T, K	298
σ^f, N/m²	$8.9\cdot 10^6$	ρ_0^s, Ns²/m⁴	$2.65\cdot 10^3$
σ^{ff}, N/m²	$8.91\cdot 10^5$	ρ_0^f, Ns²/m⁴	$9.90\cdot 10^2$
ξ^{ff}, Ns/m⁴	$4.950\cdot 10^6$	τ, sec	0.002
α_1, N/m² K²	$0.03831\cdot 10^2$	ζ^f, N/m²	$2.15\cdot 10^6$

Equations (29), (30) are solved numerically using the above numerical data and for the non-local parameters ξ_1^2 = 11, and ξ_2^2 = 4.25, as well as the impedance parameters z_1 = 0.01, z_2 = 0.02, z_3 = 0.03, z_4 = 0.04, z_5 = 0.05.

Impact of fractional order strain on phase velocity

The impact of fractional order strain on dilatational and transversal waves are shown with the help of Figs. 2–6.

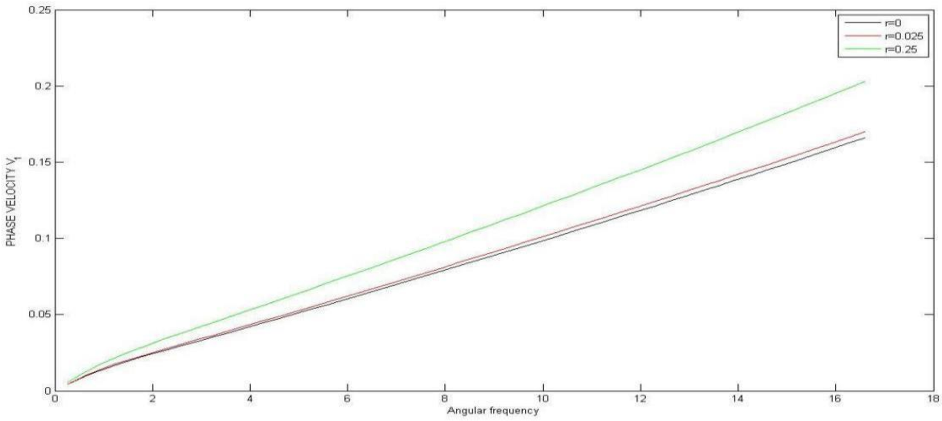

Fig. 2. Variation of longitudinal phase velocity V_1 w.r.t angular frequency

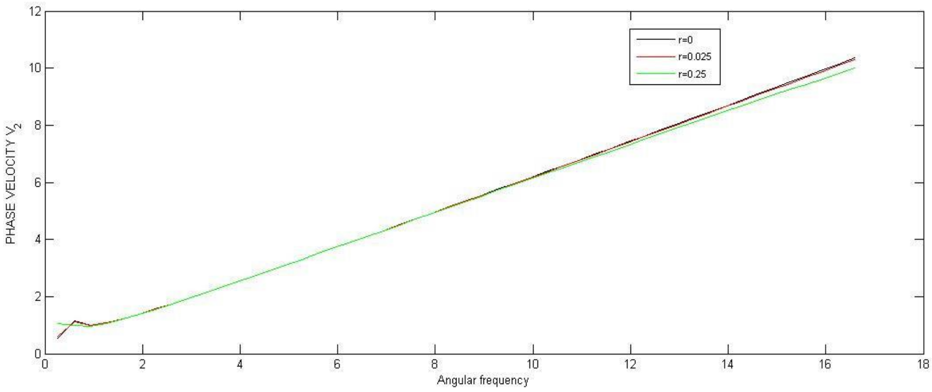

Fig. 3. Variation of longitudinal phase velocity V_2 w.r.t. angular frequency

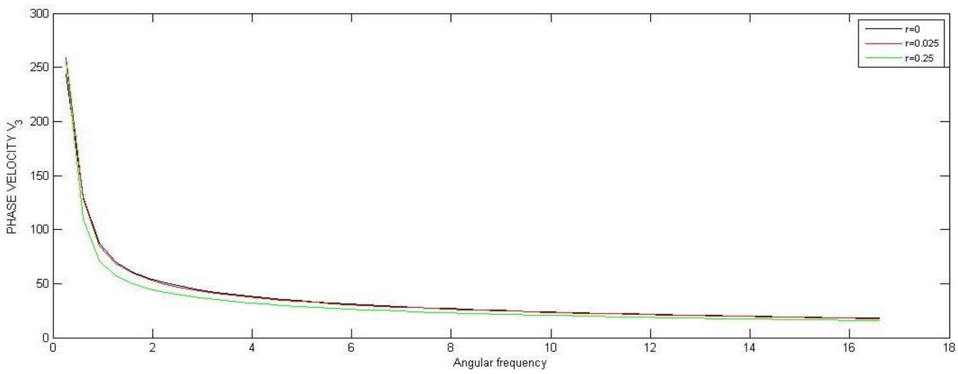

Fig. 4. Variation of longitudinal phase velocity V_3 w.r.t. angular frequency

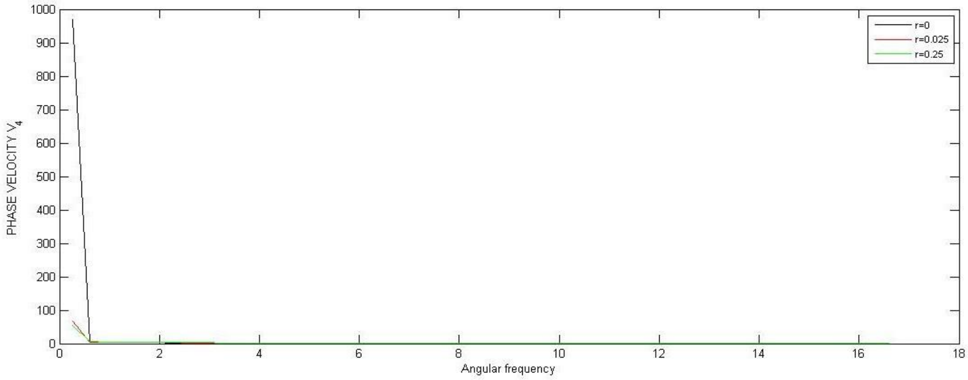

Fig. 5. Variation of transversal phase velocity V_4 w.r.t. angular frequency

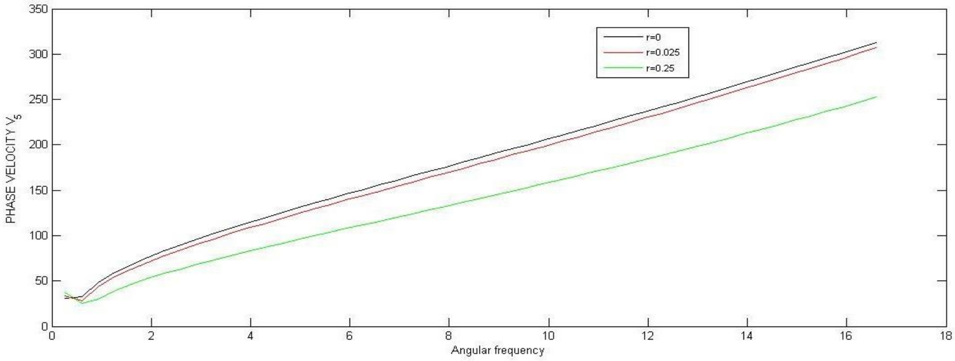

Fig. 6. Variation of transversal phase velocity V_5 w.r.t. angular frequency

Figures 2–4 shows the variation in longitudinal phase velocity w.r.t. angular frequency due to variation in fractional order strain. Figure 2 depicts that phase velocity V_1 increases with angular frequency. As values of fractional order strain is raised phase velocity V_1 also increase. From Fig. 3, it is prominent that phase velocity V_2 initially oscillates and then increase with higher values of frequency. When $r = 0.25$ velocity V_2 is greater than the velocity attained for $r = 0$ and 0.025 but for higher values of frequency opposite trend is noticed in their behavior. Impact of fractional order strain on variation of phase velocity V_3 is presented in Fig. 4. It is observed that tendency of phase velocity V_3 decrease with angular frequency and became dispersion less. Velocity V_3 decrease with higher values of fractional order strain. It is also observed that values of phase velocities for $r = 0$ and $r = 0.025$ are close to each other in entire region.

Figures 5 and 6 shows the variance in transversal velocity V_4 and V_5 w.r.t. angular frequency due to change in fractional order stain. From Fig. 5 it is noticed that values of velocity V_4 decrease with angular frequency. Initially V_4 for $r = 0$ much higher than the values acquired for $r = 0.25$ and 0.025 but its values seems to converge for for higher values of frequency. It is also detected that initially phase velocity decrease with higher values of fractional order strain but later they adverse behavior is depicted in their manner with respect to fractional order strain.

Variation of velocity V_5 with change in fractional order strain is demonstrated with the help of Fig. 6. It is observed that contrary to V_4 transverse velocity V_5 increase with frequency but decrease with higher values of r. It is also noticed that though trend of velocity V_5 for for higher values of r remain same but its values are close to each other for r = 0 and 0.025.

Energy ratios

The energy ratios for the reflected *Ps*-wave, *Pf*-wave, *T*-wave, *SVS*-wave, and *SVF*-wave are obtained and graphically presented in Figs. 7–11.

The energy ratios $|Ep|$ (p = 1, ... , 5) of these waves are plotted with respect to angle of incidence for three different values of the fractional strain parameter: r = 0, 0.025, and 0.25.

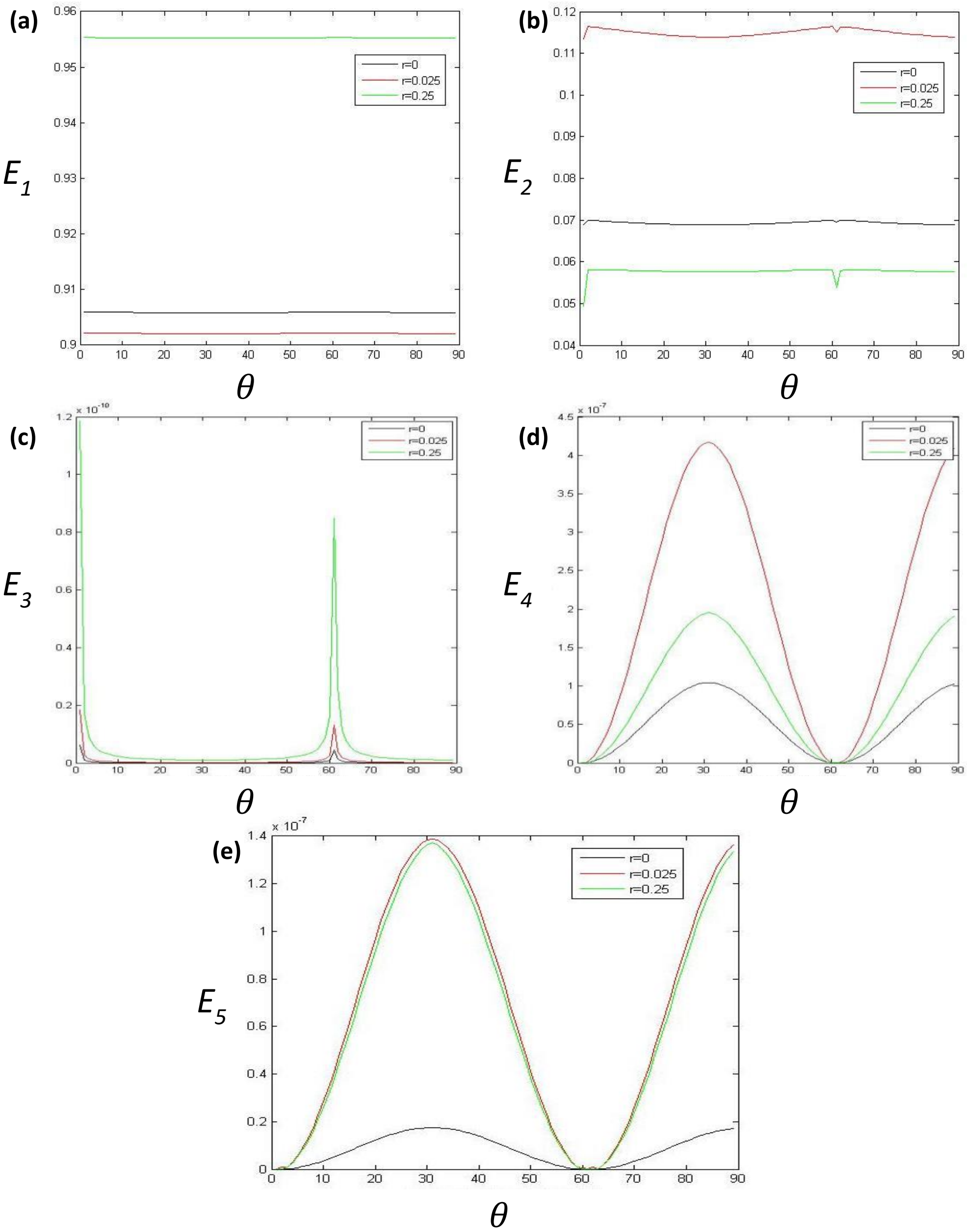

Fig. 7. Variation in energy ratios of reflected waves E for incidence of *Ps* wave in comparison of angle of incidence θ at distinct values of r: (a) E_1, (b) E_2, (c) E_3, (d) E_4, (e) E_5

The energy ratios of reflected waves when the *Ps* wave is incident are shown in Fig. 7. $|E_1|$ is found to change little with incidence angle. Also, the values of $|E_1|$ at $r = 0$ is greater than the values attained at $r = 0.025$ but less than the values acquired at $r = 0.25$. The energy ratio $|E_2|$ first rises with the angle of incidence before fluctuating somewhat in its values. As similar to Fig. 2, the values of $|E_2|$ obtained at $r = 0$ remain between the values obtained for $r = 0.025$ and $r = 0.25$. Higher values of r result in higher values of $|E_3|$ for reflected T wave values. At $\theta = 62°$ for $r = 0$, $r = 0.025$, and $r = 0.25$, there is a rise in the values of $|E_3|$, and subsequently there is a fall with angle of incidence. Energy ratio values $|E_4|$ and $|E_5|$ exhibit oscillating behavior. Both $|E_4|$ and $|E_5|$ obtain the least value at $\theta = 62°$ and maximum value at $\theta = 30°$. Values of $|E_5|$ are close to each other for $r = 0.025$, and $r = 0.25$. In comparison to other values of r, the values found for $|E_4|$ and $|E_5|$ at $r = 0$ continue to be the least.

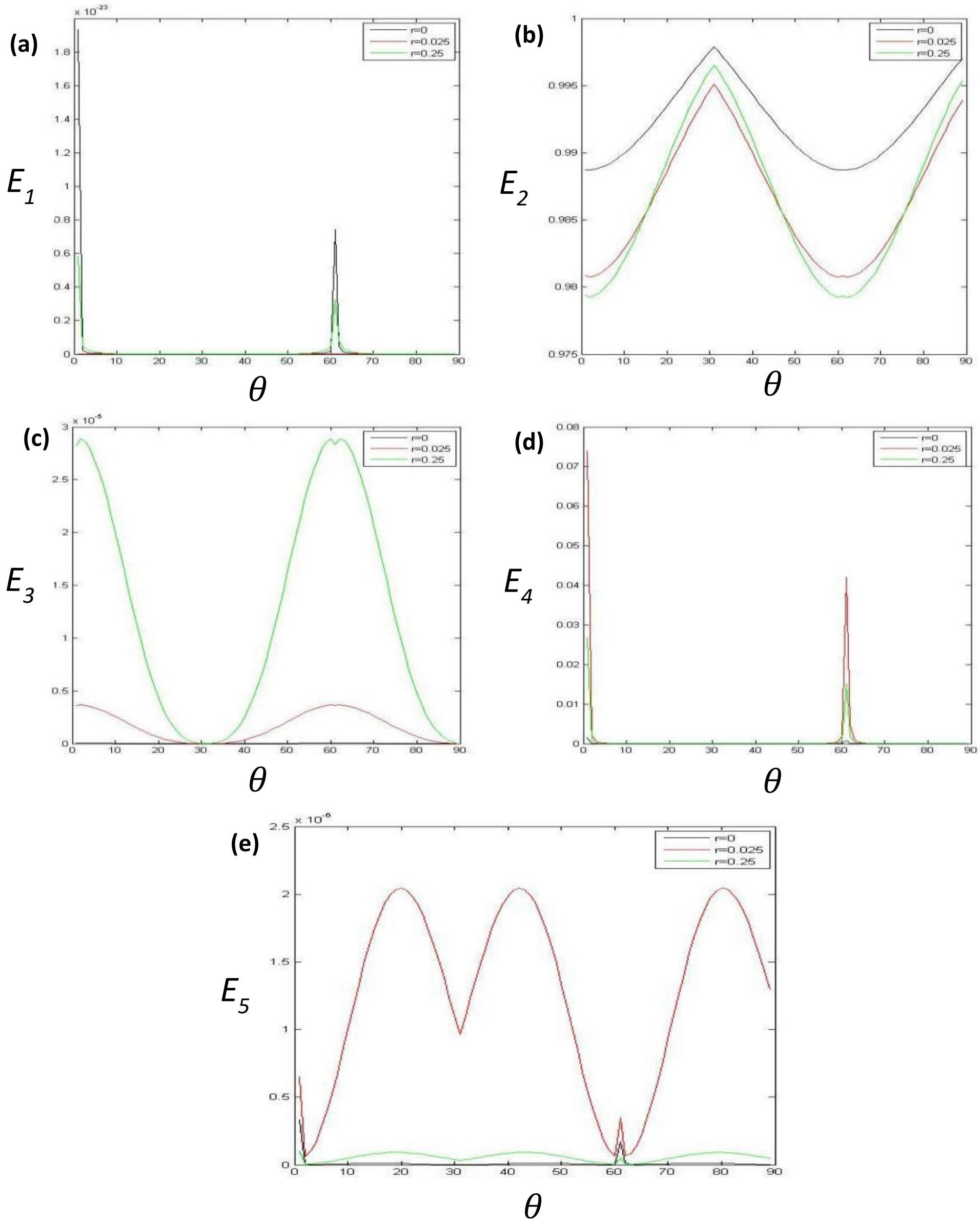

Fig. 8. Variation in energy ratios of reflected waves for incidence of *Pf* wave in comparison of angle of incidence at distinct values of r: (a) E_1, (b) E_2, (c) E_3, (d) E_4, (e) E_5

The fluctuation in energy ratios caused by *Pf* wave incidence is depicted in Fig. 8. The energy ratio, $|E_1|$, decreases in $1° \leq \theta \leq 50°$, then rises to reach its maximum value at $\theta = 62°$ before beginning to decline at higher values of θ. Additionally, it is noted that when fractional strain increases in order, $|E_1|$ values drop. The values of the energy ratio $|E_2|$ remain roughly close to one, as seen in Fig. 8(b). It slowly increases at first, then decreases, and then starts to increase again. The values of $|E_2|$ drop as fractional order strain increases, while the values of $|E_3|$ grow as fractional order strain increases. The values found for $|E_4|$ and $|E_5|$ at $r = 0$ continue to be the least and maximum at $r = 0.025$. Also, $|E_4|$ acquires a sudden rise in values at $\theta = 62°$ for all values of r. $|E_5|$ also increase at $\theta = 62°$ for $r = 0$ and 0.25 but when $r = 0.025$ it becomes least for the same value of θ.

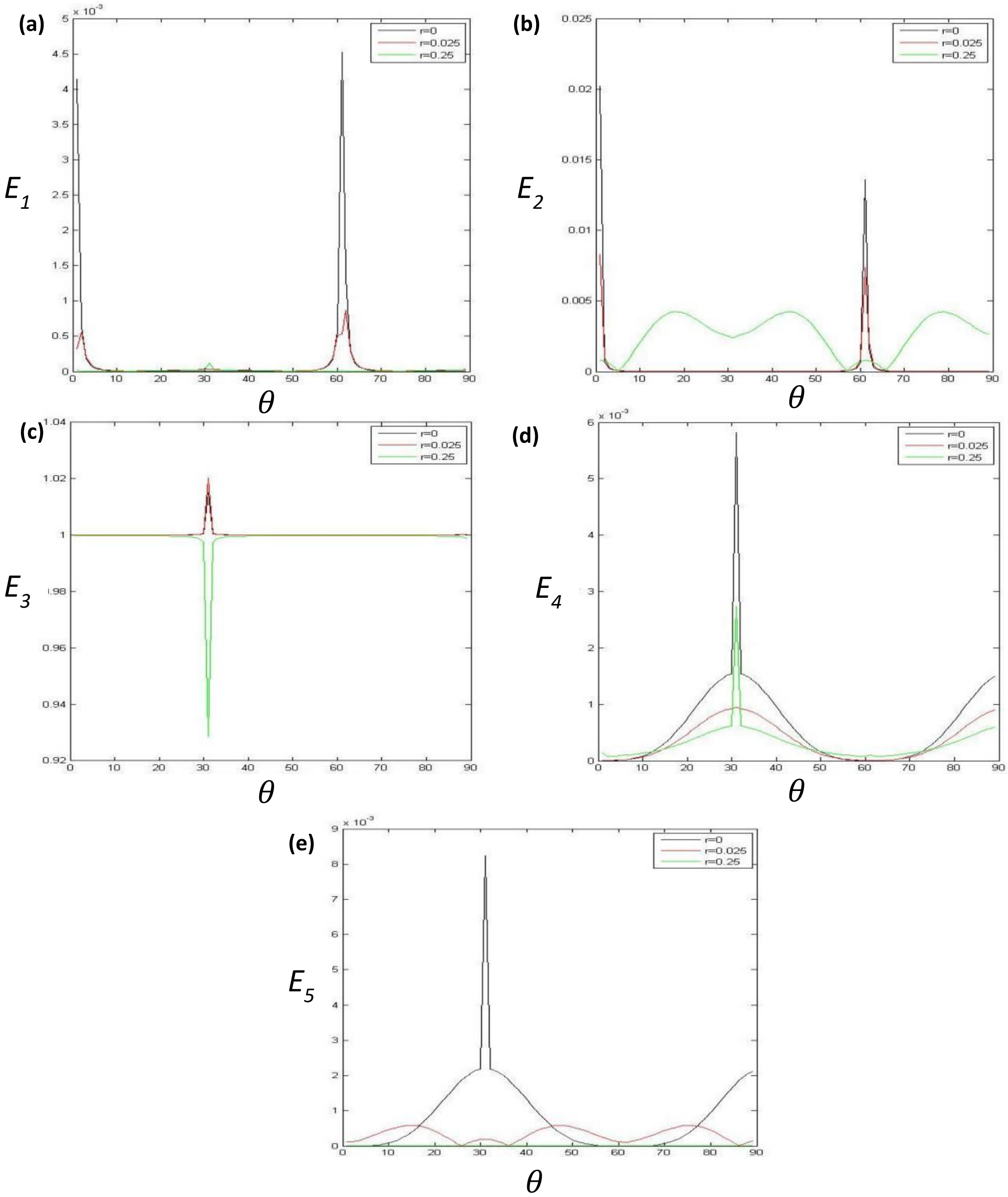

Fig. 9. Variation in energy ratios of reflected waves for incidence of *T* wave in comparison of angle of incidence at distinct values of r: (a) E_1, (b) E_2, (c) E_3, (d) E_4, (e) E_5

The energy ratios of reflected waves as a result of T wave incidence are shown in Fig. 9. It is observed that as the values of fractions order strain grow, $|E_1|$, $|E_3|$ and $|E_4|$ decrease. In the case of $r = 0$, the energy ratio $|E_2|$ decreases initially and then increases, while for $r = 0.025$, it oscillates across the whole range and reaches values that are greater than those obtained for $r = 0$ and 0.25, with the exception of $\theta = 62°$. $|E_3|$ attains highest value at $\theta = 62°$ when $r = 0$ and 0.25 but least value for $r = 0.025$. $|E_4|$ attains a peak in its values when $\theta = 30°$ for all values of fractional order strain. The values of $|E_5|$ exhibit oscillatory behavior, acquiring the lowest values at $r = 0.25$ when compared to other values of r.

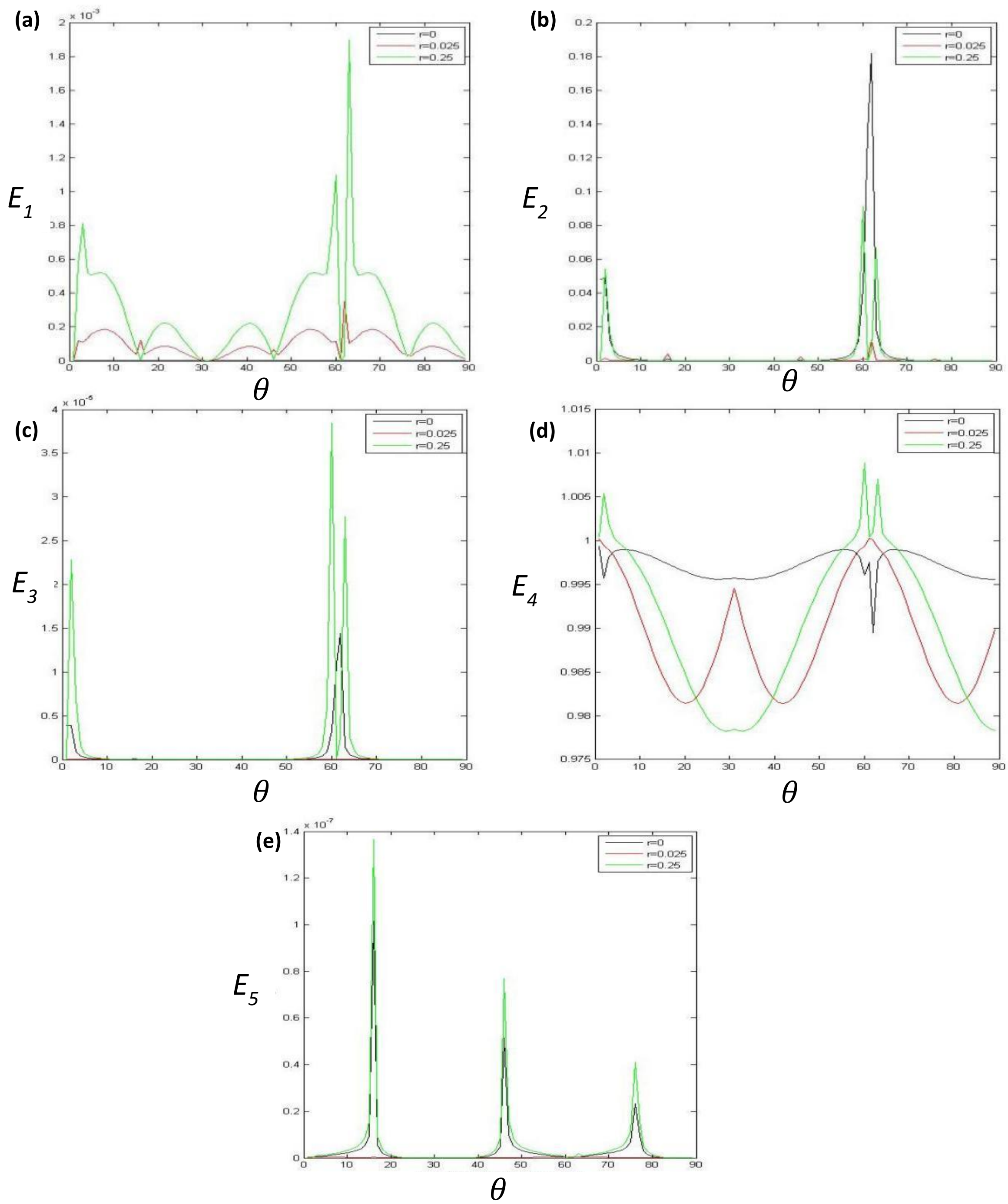

Fig. 10. Variation in energy ratios of reflected waves for incidence of *SVS* wave in comparison of angle of incidence at distinct values of r: (a) E_1, (b) E_2, (c) E_3, (d) E_4, (e) E_5

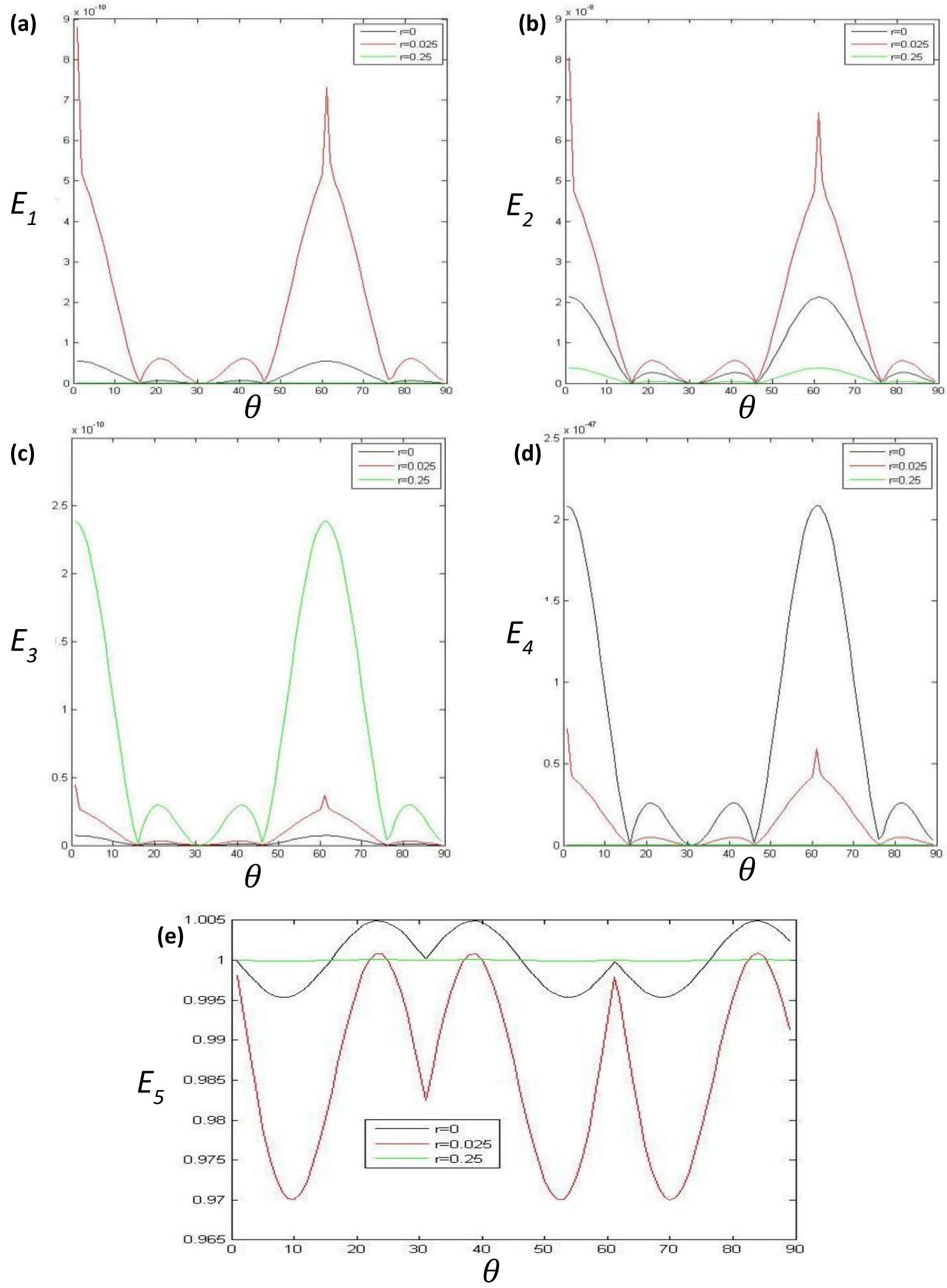

Fig. 11. Variation in energy ratios of reflected waves for incidence of *SVF* wave in comparison of angle of incidence at distinct values of r: (a) E_1, (b) E_2, (c) E_3, (d) E_4, (e) E_5

The energy ratio changes of reflected waves when *SVS* wave is incident is shown in Fig. 10. It is seen that $|E_1|$ exhibits oscillatory behavior, and its values increase with r. $|E_2|$ oscillates with angle of incidence and attains maximum values at $\theta = 62°$ for all values of r. Also values of $|E_2|$ are maximum at $r = 0$. The values of $|E_3|$ and $|E_5|$ at $r = 0$ is higher than those obtained at $r = 0.025$, but they are still lower than the values obtained at $r = 0.25$. At $\theta = 62°$, $|E_4|$ attains smallest value for $r = 0$, but highest values for $r = 0.025$ and 0.25.

The energy ratios when the *SVF* wave is incident are exhibited in Fig. 11. It is detected that reflected wave energy ratios exhibit oscillatory behaviour. At $r = 0.25$, the energy ratios $|E_1|$ and $|E_2|$ reach their minimum value and for $r = 0.025$ it acquires maximum value. While $|E_4|$ decreases as fractional strain values rise, $|E_3|$ values rise with greater values of r. For $r = 0.025$, the values of $|E_5|$ stay at their lowest at $r = 0.25$. $|E_2|$ and $|E_4|$ continue to be larger at $r = 0$ and smaller at $r = 0.025$.

Impact of swelling porosity on energy ratios

In order to depict the influence of swelling porosity on energy ratios, after substituting $\sigma^f = \xi^{ff} = \gamma^f = \mu_v = \lambda_v = \sigma^{ff} = \alpha^f = \rho_0^f = \zeta^f = 0$ in basic Eqs. (1)–(3), we get corresponding results for without swelling porous (WSP) elastic materials. In Figs. 12–14 energy ratios for swelling porous (SP) and WSP materials are obtained when *Ps* wave is incident. Here solid black line represents the graphs for swelling porous materials (SP) and the graphs in red line shows the results acquired for without swelling porous materials (WSP).

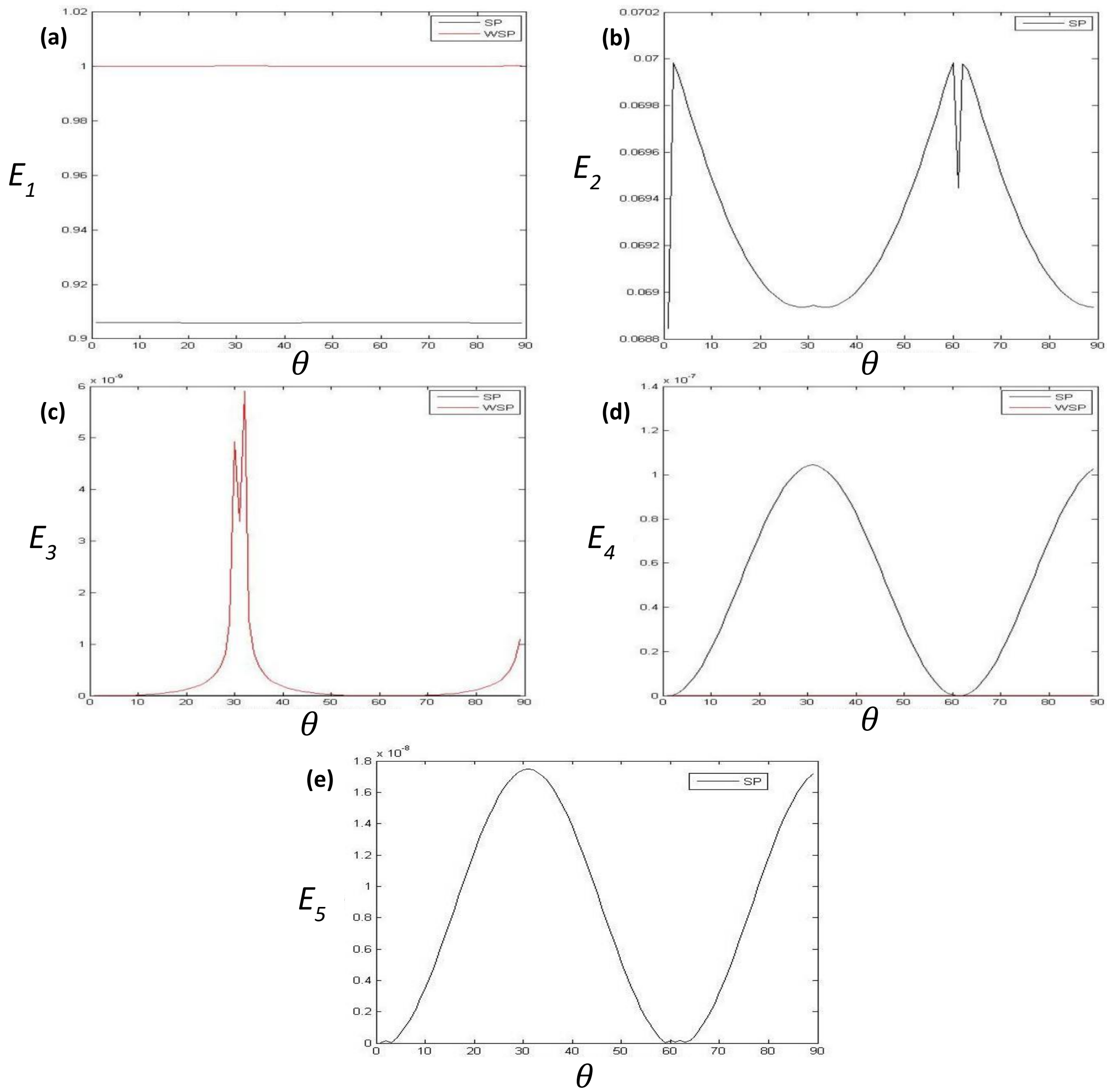

Fig. 12. Impact of swelling porosity on energy ratios when fractional order strain $r = 0$: (a) E_1, (b) E_2, (c) E_3, (d) E_4, (e) E_5

Figure 12 shows the energy ratios for SP and WSP w.r.t. angle of incidence when value of $r = 0$. Figure 12(a) demonstrates that energy ratio $|E_1|$ in both SP and WSP medium are close to one with less variation in values when *Ps* wave is incident, but its values in SP medium are less than those obtain for WSP medium for entire range. Energy ratio $|E_3|$ is of oscillatory behavior in both SP and WSP medium as shown in Fig. 12(c). Here also values of WSP medium dominates the values acquired for SP medium. Figure 12(d) depicts that $|E_4|$ keeps oscillating with angle of incidence for both the medium. In contrary to $|E_1|$ and $|E_3|$, here values in SP medium are higher than those obtain for WSP medium.
Figure 13 demonstrate the comparison between the energy ratios attained for SP and WSP medium when value of $r = 0.025$. Here again values of WSP for $|E_1|$ and $|E_3|$ are greater than the results obtained for SP materials as observed in the case for $r = 0$. Value of $|E_1|$ is approximately one for both SP and WSP medium whereas $|E_3|$ is of oscillatory

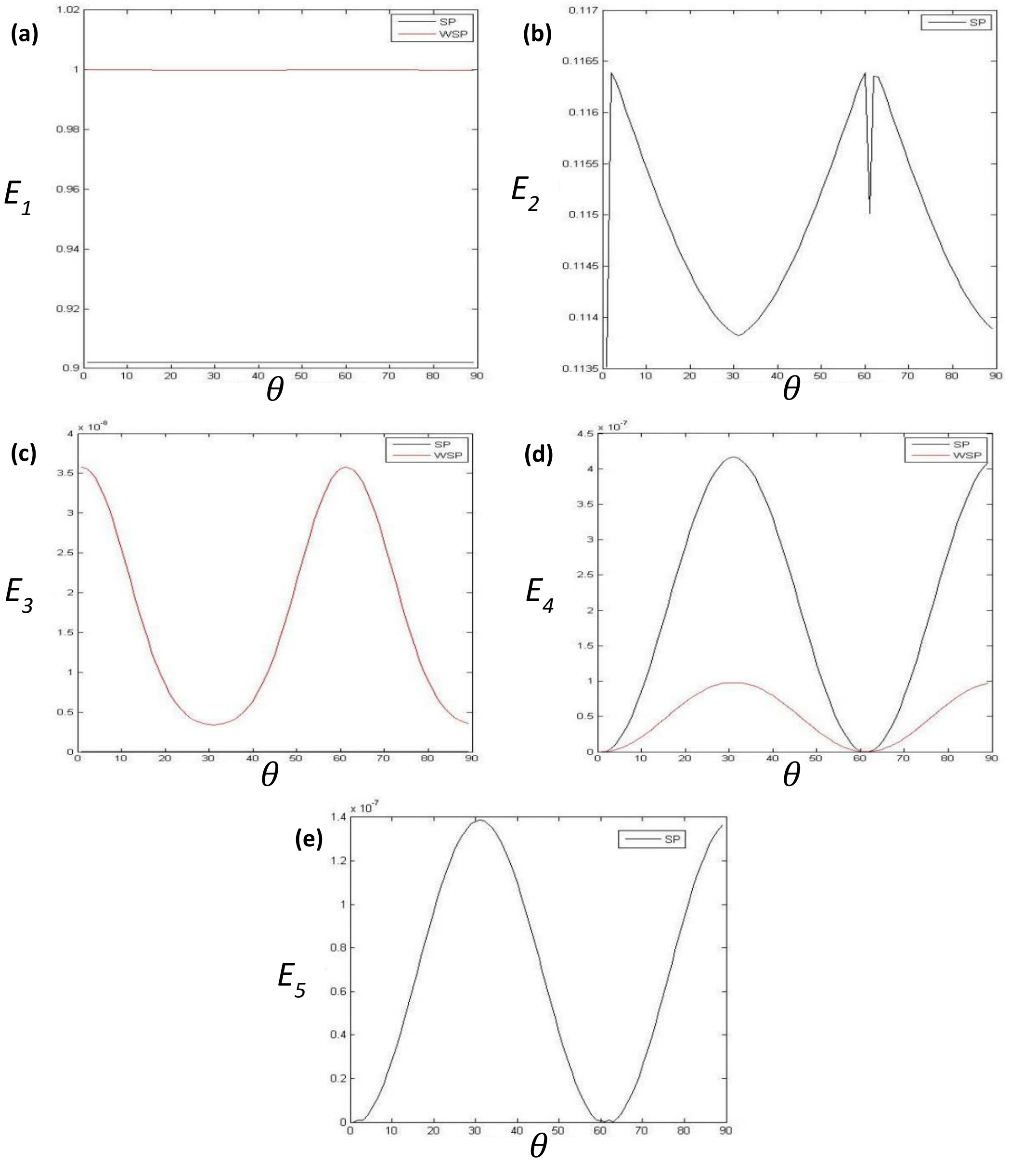

Fig. 13. Impact of swelling porosity on energy ratios when fractional order strain $r = 0.025$: (a) E_1, (b) E_2, (c) E_3, (d) E_4, (e) E_5

behavior. Figure 12(d) represents that energy ratio $|E_4|$ oscillates and obtains least value at $\theta = 62°$. Here, values in SP medium are higher than those obtained for WSP medium. It clearly shows the impact of swelling porosity of the materials.

When value of r is raised to 0.25 energy ratios obtained in SP and WSP medium are represented in Fig. 14. Figure 14(a,c) shows that here also WSP medium dominates the values obtained for SP medium as observed in case when $r = 0$ and $r = 0.025$. Figure 14(d) depicts that trend of $|E_4|$ for SP and WSP medium is same with small difference in their values. It is also noticed that the values of energy ratios $|E_4|$ obtained for WSP medium are higher than the SP medium which is contrary to the case when $r = 0$ and 0.025.

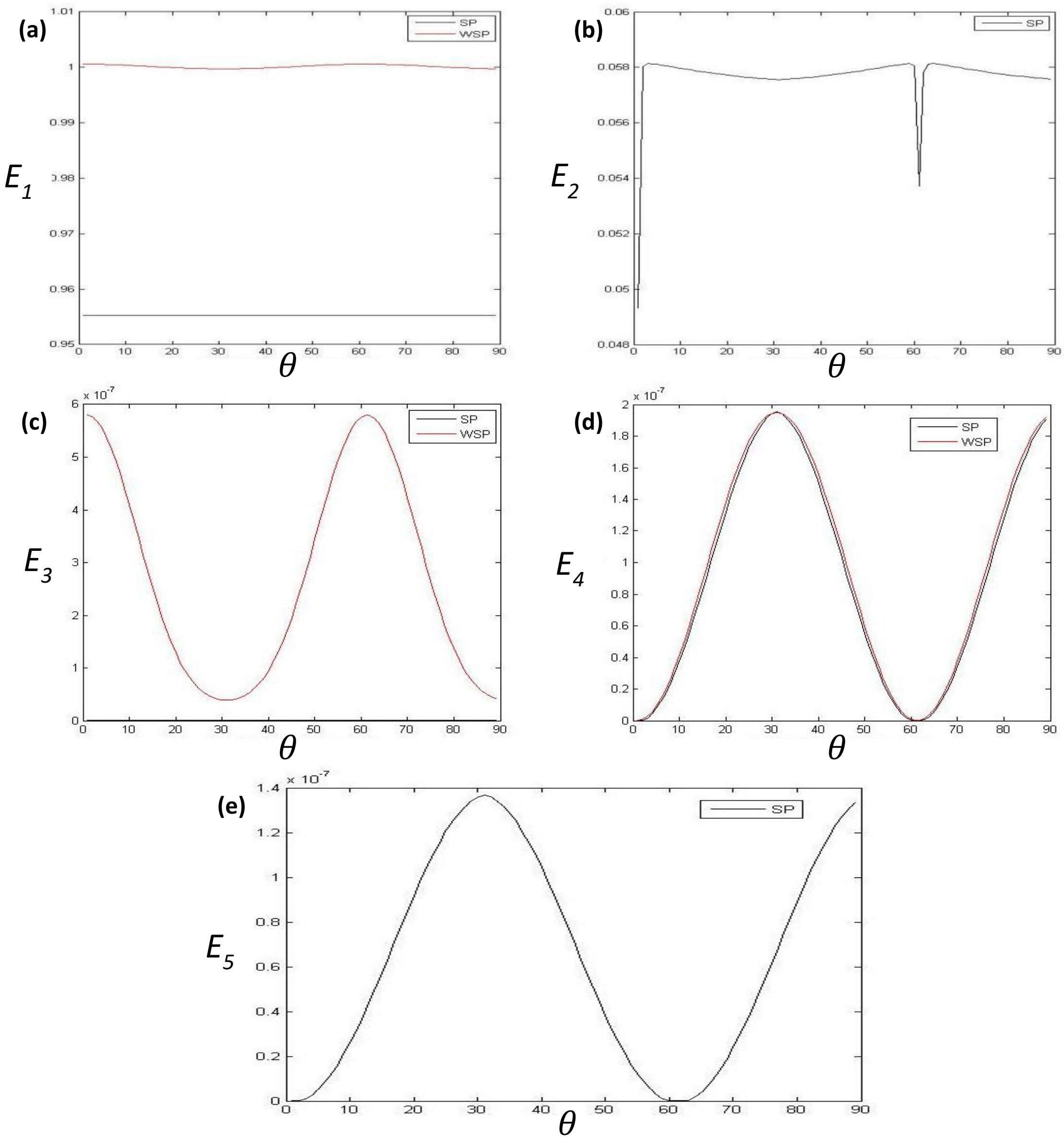

Fig. 14. Impact of swelling porosity on energy ratios when fractional order strain $r = 0.25$: (a) E_1, (b) E_2, (c) E_3, (d) E_4, (e) E_5

Conclusions

Plane wave propagation in nonlocal swelling porous thermoelastic under fractional order strain is scrutinized. It has been observed that there exist five plane waves consisting of three set of coupled longitudinal waves and two set of coupled transverse waves propagating with distinct speeds. The reflection phenomena of these waves at the impedance boundary have been examined. The expressions giving reflection coefficients and energy ratios at the stipulated boundary have been presented. The impact of fractional order strain and swelling porosity on energy ratios are obtained numerically and illustrated graphically. From the analysis of the illustrations, we derive the following conclusion: the energy ratios depend on the angle of incidence as well as the properties of the medium. The nature of dependence is distinct for distinct reflected waves. Theoretical as well as numerical results show that the energy ratios of various reflected waves are affected by fractional order strain and swelling porous parameters. Effect of nonlocal parameters is quite pertinent on the energy ratios. Phase velocity decrease with higher values of fractional order strain but *Ps* and *SVS* behaves in opposite manner. Phase velocity of thermal wave *T* and *SVS* wave decrease whereas velocity of *Ps*, *Pf* and *SVF* wave increase with angular frequency. All existing waves in stipulated medium are dominated by fractional order parameter. Energy ratios of reflected *T, SVS* and *SVF* wave are smallest for lower values of fractional order parameter when *Ps* and *Pf* wave is incident. Fractional order strain parameters decrease the energy ratios when *T* wave is encountered. Energy ratio of reflected *Ps* wave increase with fractional order strain in case of incident *SVS* wave, whereas energy ratio of reflected *T* wave decrease when *SVF* wave is incident. When longitudinal waves are incident $\theta = 62°$ behaves like a critical angle. Swelling porosity decrease the magnitude of energy ratios of *Ps* and *T* wave for all values of fractional order parameter except for *SVS* wave. In WSP medium energy ratio of reflected *Ps* and *T* wave dominates the values obtained for SP medium on contrary to that energy ratios of reflected *SVS* wave are higher in SP medium. Increase in fractional order results in dominance of WSP over SP medium. The numerical result depict that the sum of modules values of energy ratio is approximately unity at each angle of incidence. This shows that there is no dissipation of energy during reflection phenomena and hence prove the law of conservation of energy.

Application

The results proffered in this work will prove to be helpful for researchers working with material science and physicists as well as those working on the expansion of a swelling porous thermoelasticity theories. The nonlocal and fractional order strain theory of thermoelasticity has dignified applications or usages in fracture mechanics, nuclear reactors and nano-mechanics. Moreover, the nonlocal swelling porous thermoelastic under fractional order strain is more realistic than the swelling porous thermoelasticity. Wave propagation is a powerful technique to detect minerals and fluid inside the earth. The problem explored in a stipulated model engages in a significant role in various engineering fields for example civil engineering, petroleum engineering and nuclear waste management.

CRediT authorship contribution statement

Saurav Sharma Sc: writing-review and editing, conceptualization, investigation, supervision, data curation; **Divya Batra** Sc: writing-review and editing, writing-original draft, Investigation, data curation; **Rajneesh Kumar** Sc: writing-original draft, conceptualization, supervision, data curation.

Conflict of interest

The authors declare that they have no conflict of interest.

References

1. Biot MA. Theory of propagation of elastic waves in a fluid-saturated porous solid. I. Low-frequency range. *Journal of the Acoustical Society of America.* 1956;28(2): 168–178.
2. Biot MA. Theory of propagation of elastic waves in a fluid-saturated porous solid. II. Higher frequency range. *Journal of the Acoustical Society of America.* 1956;28(2): 17–191.
3. Eringen AC. A continuum theory of swelling porous elastic soils. *International Journal of Engineering Science.* 1994:32(8): 1337–1349.
4. Kumar R, Taneja D, Kumar K. Reflection and Transmission at the Boundary Surface of Thermoelastic Swelling Porous Media. *Journal of Applied Mechanical Engineering.* 2012:1(1): 1000104.
5. Magin R, Royston T. Fractional-order elastic models of cartilage: A multi-scale approach. *Communications in Nonlinear Science and Numerical Simulation.* 2010;15(3): 657–664.
6. Youssef HM. Theory of generalized thermoelasticity with fractional order strain. *Journal of Vibration and Control.* 2016:22(18): 3840–3857.
7. Chirilă A, Marin M. The theory of generalized thermoelasticity with fractional order strain for dipolar materials with double porosity. *Journal of Materials Science.* 2018;53(8): 3470–3482.
8. Youssef HM, Al-Lehaibi EA. State-space approach to three-dimensional generalized thermoelasticity with fractional order strain. *Mechanics of Advanced Materials and Structures.* 2019;26(10): 878–885.
9. Bassiouny E. Heating of thermoelastic half-space with fractional order strain and variable thermal conductivity. *Mechanics of Solids.* 2022;57(1): 163–177.
10. Al-Lehaibi EAN. Generalized Thermoelastic Infinite Annular Cylinder under the Hyperbolic Two-Temperature Fractional-Order Strain Theory. *Fractal and Fractional.* 2023;7(6): 476.
11. Sherief HH, Magdy AE. Solution of the generalized problem of thermoelasticity in the form of series of functions. *Journal of Thermal Stresses.* 1994;17(1): 75–95.
12. Ezzat MA, Othman MI, Smaan AA. State space approach to two-dimensional electromagneto–thermoelastic problem with two relaxation times. *International Journal of Engineering Science.* 2001:39(12): 1383–1404.
13. Ezzat MA. Fundamental solution in generalized magneto-thermoelasticity with two relaxation times for perfect conductor cylindrical region. *International Journal of Engineering Science.* 2004;42(13): 1503–1519.
14. Ezzat MA, El-Bary AA. State space approach of two-temperature magneto-thermoelasticity with thermal relaxation in a medium of perfect conductivity. *International Journal of Engineering Science.* 2009;47(4): 618–630.
15. El-Karamany AS, Ezzat MA. On the two-temperature Green–Naghdi thermoelasticity theories. *Journal of Thermal Stresses.* 2011;34(12): 1207–1226.
16. Vlase S, Marin M, Scutaru ML, Munteanu R. Coupled transverse and torsional vibrations in a mechanical system with two identical beams. *AIP Advances.* 2017;7(6): 065301.
17. Saurav S, Devi S, Kumar R, Marin M. Examining basic theorems and plane waves in the context of thermoelastic diffusion using a multi-phase-lag model with temperature dependence. To be published in *Mechanics of Advanced Materials and Structures.* [Preprint] 2024. Available from: doi.org/10.1080/15376494.2024.2370523.
18. Marin M, Abbas I, Kumar R. Relaxed Saint-Venant principle for thermoelastic micropolar diffusion. *Structural Engineering and Mechanics.* 2014;51(4): 651–662.
19. Sharma K. Reflection of plane waves in thermodiffusive elastic half-space with voids. *Multidiscipline Modeling in Materials and Structures.* 2012;8(3): 269–296.

20. Sharma K, Sharma S, Bhargava RR. Propagation of waves in micropolar thermoelastic solid with two temperatures bordered with layers or half spaces of inviscid liquid. *Materials Physics and Mechanics.* 2013;16(1): 66–81.
21. Sharma K, Marin M. Effect of distinct conductive and thermodynamic temperatures on the reflection of plane waves in micropolar elastic half-space. *University Politehnica of Bucharest Scientific Bulletin-Series A-Applied Mathematics and Physics.* 2013;75(2): 121–132.
22. Sharma K, Marin M. Reflection and transmission of waves from imperfect boundary between two heat conducting micropolar thermoelastic solids. *Analele Stiintifice ale Universitatii Ovidius Constanta, Seria Matematica.* 2014;22(2): 151–176.
23. Vinh PC, Hue TTT. Rayleigh waves with impedance boundary conditions in incompressible anisotropic half-spaces. *International Journal of Engineering Science.* 2014; 85: 175–185.
24. Kumar R, Sharma P. Some theorems and wave propagation in a piezothermoelastic medium with two-temperature and fractional order derivative. *Materials Physics and Mechanics.* 2021;47(2): 196–218.
25. Sharma S, Khator S. Power generation planning with reserve dispatch and weather uncertainties including penetration of renewable sources. *International Journal of Smart Grid and Clean Energy.* 2021;10(4): 292–303.
26. Sharma S, Khator S. Micro-Grid Planning with Aggregator's Role in the Renewable Inclusive Prosumer Market. *Journal of Power and Energy Engineering.* 2022;10(4): 47–62.
27. Kumar R, Kaushal S, Kochar A. Response of impedance parameters on waves in the micropolar thermoelastic medium under modified Green-Lindsay theory. *ZAMM Journal of applied mathematics and mechanics: Zeitschrift fuŕ angewandte Mathematik und Mechanik.* 2022;102(9): 202200109.
28. Singh B, Kaur B. Rayleigh surface wave at an impedance boundary of an incompressible micropolar solid half-space. *Mechanics of Advanced Materials and Structures.* 2022;29(25): 3942–3949.
29. Amin MM, Hendy MH, Ezzat MA. Wave propagation due to laser irradiation in viscoelastic thin metal film with fractional relaxation operator. *Materials Physics and Mechanics.* 2022;48(1): 30–43.
30. Kaushal S, Kumar R, Kochar A. Wave propagation under the influence of voids and non-free surfaces in a micropolar elastic medium. *Materials Physics and Mechanics.* 2022;50(2): 226–238.
31. Ezzat MA, Lewis RW. Two-dimensional thermo-mechanical fractional responses to biological tissue with rheological properties. *International Journal of Numerical Methods for Heat & Fluid Flow.* 2022;32(6); 1944–1960.
32. Amin MM, Hendy MH, Ezzat MA. Wave propagation due to laser irradiation in viscoelastic thin metal film with fractional relaxation operator. *Materials Physics and Mechanics.* 2022;48(1): 30–43.
33. Ezzat MA, Al-Muhiameed ZIA. Thermo-mechanical response of size-dependent piezoelectric materials in thermo-viscoelasticity theory. *Steel and Composite Structures.* 2022;45(4): 535–546.
34. Ezzat MA, Ezzat SM, Alkharraz MY. State-space approach to nonlocal thermo-viscoelastic piezoelectric materials with fractional dual-phase lag heat transfer. *International Journal of Numerical Methods for Heat & Fluid Flow.* 2022;32(12): 3726–3750.
35. Ezzat MA, Ezzat SM, Alduraibi NS. On size-dependent thermo-viscoelasticity theory for piezoelectric materials. To be published in *Waves in Random and Complex Media.* [Preprint] 2022. Available from: doi.org/10.1080/17455030.2022.2043569.
36. Yadav AK, Carrera E, Schnack E, Marin M. Effects of memory response and impedance barrier on reflection of plane waves in a nonlocal micropolar porous thermo-diffusive medium. *Mechanics of Advanced Materials and Structures.* 2023;31(22): 5564–5580.
37. Senthilkumar V. Fractional derivative analysis of wave propagation studies using Eringen's nonlocal model with elastic medium support. *Journal of Vibration Engineering & Technologies.* 2023;11(8): 3677–3685.
38. Abouelregal AE, Marin M, Öchsner A. The influence of a non-local Moore–Gibson–Thompson heat transfer model on an underlying thermoelastic material under the model of memory-dependent derivatives. *Continuum Mechanics and Thermodynamics.* 2023;35(2): 545–562.
39. Abouelregal AE, Marin M, Askar SS, Foul A. A non-local fractional two-phase delay thermoelastic model for a solid half-space whose properties change with temperature and affected by hydrostatic pressure. *ZAMM Journal of applied mathematics and mechanics: Zeitschrift fuŕ angewandte Mathematik und Mechanik.* 2024;104(8): e202400102.
40. Alsaeed SS, Abouelregal AE, Elzayady ME. Magneto-thermoelastic responses in an unbounded porous body with a spherical cavity subjected to laser pulse heating via an Atangana-Baleanu fractional operator. *Case Studies in Thermal Engineering.* 2024;61: 104968.

41. Abouelregal AE, Civalek O, Akgöz B. A Size-Dependent Non-Fourier Heat Conduction Model for Magneto-Thermoelastic Vibration Response of Nanosystems. To be published in *Journal of Applied and Computational Mechanics.* {Preprint] 2024. Available from: doi.org/10.22055/jacm.2024.46746.4584.
42. Kaushal S, Kumar R, Bala I, Sharma G. Impact of non-local, two temperature and impedance parameters on propagation of waves in generalized thermoelastic medium under modified Green-Lindsay model. *Materials Physics and Mechanics.* 2024;52(1): 1–17.
43. Ezzat MA, El-Bary AA. Analysis of thermoelectric viscoelastic wave characteristics in the presence of a continuous line heat source with memory dependent derivatives. *Archive of Applied Mechanics.* 2023;93(2): 605–619.
44. Yadav AK. Reflection of plane waves from the impedance boundary of a magneto-thermo-microstretch solid with diffusion in a fractional order theory of thermoelasticity. *Waves in Random and Complex Media.* 2024;34(1): 404–433.
45. Elhagary MA. Thermoelastic diffusion in a half space due to fractional order theory. *Waves in Random and Complex Media.* 2024: 1–23.
46. Alruwaili AS, Hassaballa AA, Hendy MH, Ezzat MA. New insights on fractional thermoelectric MHD theory. *Archive of Applied Mechanics.* 2024;94: 1613–1630.
47. Kumar R, Batra D, Saurav S. Thermoelastic medium with swelling porous structure and impedance boundary under dual phase lag. *Engineering Solid Mechanics.* 2025;13: 81–92.
48. Achenbach JD. *Wave Propagation in Elastic Solids.* Amsterdam: Elsevier; 1973.